THE ASTROPHYSICAL JOURNAL, 522:397–412, 1999 September 1

RXTE OBSERVATIONS OF 0.1–300 Hz QUASI-PERIODIC OSCILLATIONS IN THE MICROQUASAR GRO J1655−40

RONALD A. REMILLARD AND EDWARD H. MORGAN
Center for Space Research, Massachusetts Institute of Technology, Room 37-595, Cambridge MA 02139; rr@space.mit.edu.edu, ehm@space.mit.edu
JEFFREY E. MCCLINTOCK
Harvard-Smithsonian Center for Astrophysics, 60 Garden Street, Cambridge MA 02138; jem@cfa.harvard.edu
CHARLES D. BAILYN
Department of Astronomy, Yale University, P.O. Box 208101, New Haven, CT 06520; bailyn@astro.yale.edu
AND
JEROME A. OROSZ
Department of Astronomy and Astrophysics, Pennsylvania State University, 525 Davey Laboratory, University Park, PA 16802; orosz@astro.psu.edu
Received 1998 June 2; accepted 1999 April 12

ABSTRACT

We have investigated 52 *Rossi X-Ray Timing Explorer* pointed observations of GRO J1655−40 spanning the X-ray outburst that commenced on 1996 April 25 and lasted for 16 months. Our X-ray timing analyses reveal four types of quasi-periodic oscillations (QPOs): three with relatively stable central frequencies near 300, 9, and 0.1 Hz, and a fourth QPO that varied over the range 14–28 Hz. The 300 and 0.1 Hz QPOs appear only when the power-law component dominates the X-ray spectrum and the estimated unabsorbed X-ray luminosity is above $\sim 0.2 L_{\rm Edd}$. At lower luminosity ($L_{\rm X} \sim 0.1 L_{\rm Edd}$), the thermal component dominates the spectrum; the disk appears somewhat cooler (~ 1.3 keV), and its inner radius appears larger. In this state only two of the QPOs are observed: the broad and spectrally "soft" 9 Hz QPO and the narrow, "hard" QPO that varies from 14 to 28 Hz as the hard flux decreases. At still lower luminosities ($L_{\rm X} < 0.1 L_{\rm Edd}$), the power-law component contributes less than 30% of the total luminosity, the inner disk appears both larger and cooler, the 9 Hz QPO vanishes, and only a very weak (rms 0.3%) and narrow QPO at 28 Hz remains. The 300 Hz QPO is likely to be analogous to the stationary QPO at 67 Hz seen in the microquasar GRS 1915+105. We discuss four models of these high-frequency QPOs that depend on effects due to general relativity. The models suggest that these rapid QPOs may eventually provide a measure of the mass and rotation of the accreting black hole. The 9 Hz QPO displays a spectrum consistent with a thermal origin, but this frequency is not uniquely consistent with any of the natural timescales associated with the disk. The mechanism for the 14–28 Hz QPOs appears to be linked to the power-law component, similar to the 1–10 Hz QPOs in GRS 1915+105. Thus these low-frequency QPOs have the potential to lead us to the origin of the energetic electrons that radiate the power-law spectral component. Finally, we show data for GRO J1655−40 and GRS 1915+105 as each source teeters between relative stability and a state of intense oscillations at 0.1 Hz. A comparison of the respective spectral parameters allows us to speculate that the black hole mass in GRS 1915+105 is very large, possibly $\sim 100\ M_{\odot}$.

Subject headings: black hole physics — stars: individual (GRO J1655−40) — stars: oscillations — X-rays: stars

1. INTRODUCTION

The black hole binary GRO J1655−40 is one of the rare Galactic X-ray sources (along with GRS 1915+105 and possibly Cyg X-3) known to produce relativistic radio jets (Mirabel & Rodriguez 1994; Tingay et al. 1995; Hjellming & Rupen 1995; Mioduszewski et al. 1997; Newell, Garrett, & Spencer 1998). These jet sources and a few other Galactic X-ray sources that exhibit double-lobed radio structure (e.g., 1E 1740.7−2942; see Smith et al. 1997 and references therein) are collectively referred to as "microquasars," since they have properties analogous to radio-loud active galactic nuclei. Investigations of microquasars provide opportunities to search for the cause of relativistic jets, to probe the properties of accreting black holes and their mass-donor companion stars, and to measure the spectral evolution associated with the various accretion states. GRO J1655−40 is an especially important target for such studies, since its distance and black hole mass are well established: $d \sim 3.2$ kpc has been inferred from radio absorption features (Tingay et al. 1995; McKay & Kesteven 1994), and $M_1 \sim 7\ M_{\odot}$ has been derived from optical investigations of the binary system (Orosz & Bailyn 1997; Shahbaz et al. 1999).

GRO J1655−40 was discovered with BATSE on 1994 July 27. For about 4 months thereafter, a correlation between hard X-ray outbursts (20–100 keV) and radio flares was observed, and this established a relationship between jet formation and hard X-ray activity (Harmon et al. 1995). However, there were additional hard X-ray outbursts during 1994–1995 with diminishing responses at radio frequencies (Tavani et al. 1996). Thus jet formation in GRO J1655−40 depends on some unknown factor(s) in addition to hard X-ray outbursts.

The X-ray spectrum of GRO J1655−40 has been detected with OSSE to photon energies near 1 MeV (Kroeger et al. 1996; Tomsick et al. 1999). Above 50 keV, the spectrum is consistent with a power-law function and a photon index in the range of 2.4–2.8. Soft X-ray obser-

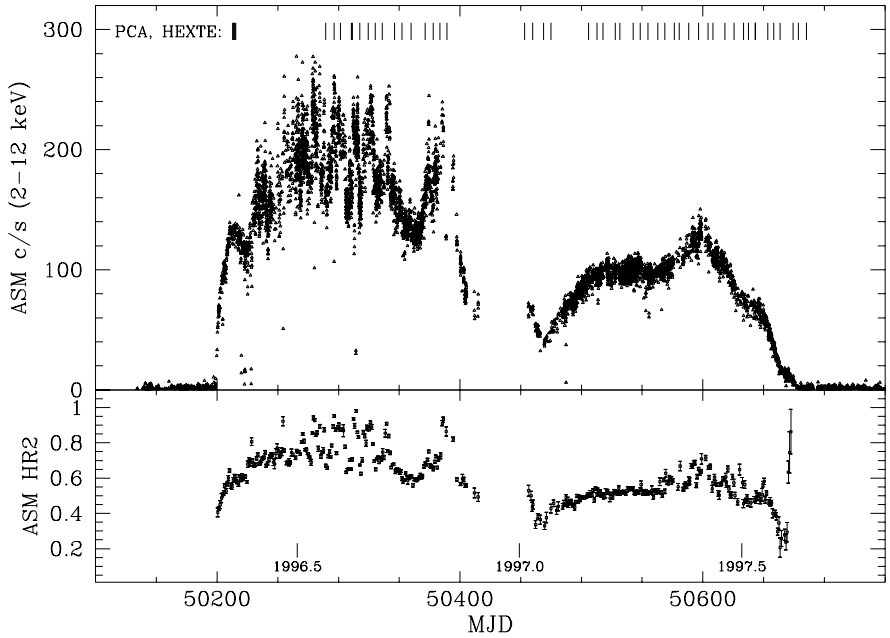

FIG. 1.—*RXTE* ASM light curves and hardness ratio covering the 1996–1997 X-ray outburst of GRO J1655−40. For reference, the count rate for the Crab Nebula is 75.5 ASM counts s^{-1}. The ASM HR2 value is the ratio of source counts at 5–12 keV relative to the counts at 3–5 keV. The tick marks in the upper portion of the top panel indicate the times of *RXTE* pointed observations considered in this paper.

vations were made with *ROSAT* during 1994 August (Greiner, Predehl, & Pohl 1995) and with *ASCA* during 1994 August–September and 1995 August (Ueda et al. 1998). Below 10 keV, the spectrum is dominated by a component that is attributed to thermal emission from the inner accretion disk. The detected flux (2–10 keV) was in the range of (0.2–4.7) $\times$ 10^{-8} ergs cm^{-2} s^{-1}, with a suggestion of persistence in soft X-rays during the times between hard X-ray outbursts.

Spectral fits for the thermal X-ray component suggest that the inner disk in GRO J1655−40 appears to be relatively small and hot, compared with the disks of other black hole binaries. A nonrotating 7 $M_\odot$ black hole would be expected to have an inner disk larger than the innermost stable orbit of $6GM_1/c^2$ or 62 km, while a rapidly rotating (prograde) black hole may have a last stable orbit as small as $1GM_1/c^2$ or 10 km (see Zhang, Cui, & Chen 1997 and references therein). Using X-ray spectral parameters with corrections for the effects of scattering and inner disk emissivity modifications expected in general relativity (GR), Zhang et al. (1997) estimated that the black hole in GRO J1655−40 is rotating at ~93% of the maximum rate. While the accuracy of this technique is subject to systematic uncertainties (see Sobczak et al. 1999), there are continuing investigations as to whether rapid rotation may be a distinguishing characteristic of the black holes in microquasars.

During late 1995 and early 1996, GRO J1655−40 entered a very low or quiescent accretion state (e.g., Ueda et al. 1998), permitting a clear optical view of the companion star. This allowed Orosz & Bailyn (1997) to improve the determinations of the binary period (2.62 days) and the spectral type of the secondary (F4 IV). They further modeled the "ellipsoidal variations" of the secondary star and the partial eclipses of the accretion disk during outburst, providing a good fit for the binary inclination angle (69°.5; see also van der Hooft et al. 1998). Shahbaz et al. (1999) improved the measurement of the binary mass function (2.73 $M_\odot$) and the mass ratio ($M_1/M_2 = 2.6$), from which they deduce a black hole mass of 6.7 ± 1.2 $M_\odot$. This is currently the only microquasar for which there is a clear understanding of the masses and dimensions of the binary system.

The All-Sky Monitor (ASM) aboard the *Rossi X-Ray Timing Explorer* (*RXTE*) began regular monitoring of the X-ray sky at 2–12 keV in early 1996. For the first 2 months of ASM observations, the source was quiescent and not detected. Then on 1996 April 25 a new outburst was discovered (Remillard et al. 1996). With great fortune, concurrent optical monitoring was in progress, and it was determined that optical brightening preceded the X-ray turn-on by 6 days, beginning first in the *I* band and then occurring sequentially in the *R*, *V*, and *B* bands (Orosz et al. 1997). These results were interpreted as evidence favoring a two-zone accretion flow consisting of a cold outer disk and an extremely hot inner disk with an advection-dominated accretion flow (Hameury et al. 1997).

Herein we report the results of X-ray timing investigations derived from a series of 52 *RXTE* pointed observations of GRO J1655−40 covering the 1996–1997 outburst. A brief and preliminary account of these results has been reported previously (Remillard et al. 1998). We describe four types of transient quasi-periodic oscillations (QPOs) in X-rays that span 0.1–300 Hz. Three of these QPO types appear only when the luminosity of the hard power-law component is high. Moreover, the 300 Hz QPO is seen only when the power-law component dominates the spectrum, and the total X-ray luminosity exceeds ~20% of the Eddington limit ($L_{\rm Edd}$). This fast QPO appears to be analogous to the stationary 67 Hz QPO seen in GRS 1915+105 (Morgan, Remillard, & Greiner 1997; Remillard & Morgan 1998).

2. OBSERVATIONS WITH THE *RXTE* ASM

The *RXTE* ASM scans the celestial sphere roughly 5 times per day. Each of its three cameras contains a position-sensitive proportional counter that is mounted below a coded mask. The typical sensitivity for measurements averaged over 1 day is ~ 7 mcrab at 3 σ significance over the full energy range of the instrument. Data in the form of position histograms are accumulated in three energy channels: 1.5–3.0, 3–5, and 5–12 keV. The mask shadow patterns are deconvolved to yield X-ray source intensities, which are then normalized to the response characteristics of camera 1. Further details regarding the instrument and data analysis methods are described by Levine et al. (1996).

The ASM light curve for GRO J1655−40 is shown in Figure 1. The times are given in modified Julian date, which is defined as MJD = JD − 2,400,000.5. The top panel displays the X-ray count rate at 2–12 keV; the vertical lines above the data points indicate the times of *RXTE* pointed observations addressed in this paper. As shown in § 4, the hard X-ray component is usually sufficiently steep that the 2–12 keV count rate is a fairly good representation of the overall X-ray luminosity. The bottom panel of Figure 1 shows measurements of the spectral hardness ratio, HR2, which is defined as the ASM count rate at 5–12 keV relative to the rate at 3–5 keV. The overall profile of this outburst in GRO J1655−40 is markedly different from the fast rise and slow exponential decay of many X-ray novae (Chen, Shrader, & Livio 1997). Here the first wave in X-ray brightness lasts for about 270 days, evolving from a soft spectral state into a hard, flaring state. The highest flux during the flares (285 counts s^{-1}) corresponds to an X-ray luminosity (unabsorbed) near 2×10^{38} ergs s^{-1} at 2–12 keV, which is $\sim 0.25 L_{\rm Edd}$ for GRO J1655−40. The isolated low points in the ASM light curve have been shown to be associated with absorption dips that occur in a narrow range of binary phase (Kuulkers et al. 1998).

After MJD 50400, the X-ray flux decreases while the spectrum softens, reaching a local minimum near MJD 50460. However, this evolution is interrupted by a second wave in brightness that extends the outburst for another 200 days. The second maximum also displays an interval of increased variability and spectral hardening. However, compared with the first maximum, the intensity is substantially lower, and the flaring is subdued. The decay from the second maximum is again associated with spectral softening. However, beginning at MJD 50,670 (1997 August 10), at a count rate of 12 counts s^{-1} (or only $0.01 L_{\rm Edd}$), the spectrum abruptly hardens again. The flux continues to decay, and on MJD 50,681 (1997 August 21) the source falls below the ASM detection limit (3 σ upper limits, ~ 9 mcrab per 1 day bin). The ASM results provide a thorough context for the analysis and interpretation of the *RXTE* pointed observations reported below. Beyond the results shown in Figure 1, there have been no further ASM detections of GRO J1655−40 through the end of 1998 (MJD 51,178).

3. PCA POWER SPECTRA OF GRO J1655−40

The central theme of this paper is an X-ray timing analysis of a series of 52 observations with the *RXTE* Proportional Counter Array (PCA). The instrument is described by Jahoda et al. (1996). The PCA consists of five xenon-filled detectors with a total collecting area ~ 6200 cm^2 at 5 keV, sensitivity in the range of 2–60 keV, and $\sim 17\%$ energy resolution at 5 keV. Depending on the observing modes chosen for a particular observation, the time resolution may be as fine as 1 μs.

The PCA observation times are listed in Table 1; they are distributed throughout the 1996–1997 outburst, as shown in Figure 1. Table 1 also provides exposure times, the number of detector units (PCUs) that were collecting data, and the PCA observing modes. The data in this study include all of the observations in our AO-1 guest observer program (P10255) and also the observations for the AO-2 public archive (P20402), except for those data obtained after MJD 50,685 (1997 August 25) when the source intensity was below 1 mcrab. With one exception, we define an observation as the collection of PCA data obtained on any one particular UT day. On 1996 November 2, GRO J1655−40 changed its intensity and QPO properties significantly between intervals of good exposure time, and we therefore divided these data into two observations labeled "A" and "B," respectively (see Table 1).

In Table 2 we provide a variety of measurements that describe the X-ray emission properties of GRO J1655−40. These include the PCA count rates for three energy bands (cols. [3], [7], and [8]), the standard deviation of the full PCA count rate (effectively 2–25 keV) in 1 s bins (col. [4]), two types of PCA hardness ratios (cols. [5] and [6]), and QPO frequencies and comments relevant to the observations (col. [9]). These results will be used below to help evaluate the conditions under which the different types of QPOs appear.

3.1. *Power Spectra for Individual Observations*

In Figures 2–4 we show the power spectra for each of the 52 PCA observations of GRO J1655−40, and the results are shown in logarithmically sampled frequency bins. We have subtracted the power due to counting statistics, with corrections for instrument dead time and electrical recovery from very large events, as described by Morgan et al. (1997). These dead-time corrections to the Poisson noise use a model for "paralyzable" effects in the detector. The power spectra are normalized to the square of the fractional rms amplitude per hertz. Since the instrument, in fact, operates with a combination of paralyzable and nonparalyzable interruptions (Zhang et al. 1995), the inaccuracies in our dead-time corrections may be seen as residual broadband power at high frequencies with a power density $\lesssim 10^{-6}$ Hz^{-1}.

All of the power spectra in Figures 2–4 show intrinsic source variations in GRO J1655−40. The broadband power continuum typically decreases with frequency in a manner roughly described as a power law with an index of 1.2 (± 0.3). Frequently there is very broad curvature in this continuum in the log power versus log frequency plane, extending from 0.1 to 10 Hz with an excess centered near 1 Hz. During many observations, we also see QPOs in the range of 7–28 Hz. The profiles of these QPOs are complex. In several cases (see panels 07/25/96, 08/16/96, 08/22/96, 09/04/96, 09/09/96, 10/27/96), the profiles suggest separate broad and narrow QPOs, with the latter found at higher frequency. Furthermore, there are two occasions (8/01/96 and 11/02/96B) in which there is an additional low-frequency QPO near 0.1 Hz.

During the final decay of GRO J1655−40 in 1997 August (after MJD 50,663), the power continuum abruptly increases and flattens, and there are renewed QPOs with

TABLE 1

OBSERVATIONS OF GRO J1655−40 WITH *RXTE*

Observation	MJD Start	MJD End	UT Date	Number of PCUs[a]	Exposure	Modes[b]
1	50212.670	50212.951	05/09/96	3.0	10122	a
2	50213.385	50213.618	05/10/96	3.0	11429	a
3	50214.318	50214.685	05/11/96	3.0	14039	b
4	50215.279	50215.618	05/12/96	3.0	14016	b
5	50289.355	50289.491	07/25/96	5.0	7430	b
6	50296.311	50296.506	08/01/96	4.0	8903	b
7	50301.664	50301.789	08/06/96	5.0	6335	b
8	50310.599	50310.678	08/15/96	4.0	3415	b
9	50311.390	50311.412	08/16/96	5.0	1895	b
10	50317.441	50317.548	08/22/96	5.0	6153	b
11	50324.379	50324.473	08/29/96	4.0	4927	b
12	50330.253	50330.353	09/04/96	5.0	6189	b
13	50335.912	50336.026	09/09/96	5.0	8164	b
14	50346.194	50346.299	09/20/96	5.0	6438	b
15	50352.197	50352.333	09/26/96	5.0	6599	b
16	50359.563	50359.741	10/03/96	4.6	5426	b
17	50371.421	50371.579	10/15/96	4.7	5385	b
18	50378.081	50378.213	10/22/96	5.0	6887	b
19	50383.564	50383.717	10/27/96	4.0	6265	b
20	50389.217	50389.257	11/02/96A	5.0	3457	b
21	50389.288	50389.324	11/02/96B	5.0	3015	b
22	50453.331	50453.428	01/05/97	5.0	6551	c
23	50460.002	50460.130	01/12/97	5.0	6536	c
24	50468.994	50469.101	01/20/97	5.0	6912	c
25	50474.822	50474.951	01/26/97	5.0	5885	c
26	50505.814	50505.979	02/26/97	5.0	9638	c
27	50512.758	50512.858	03/05/97	5.0	5884	c
28	50517.688	50517.790	03/10/97	4.0	5831	c
29	50527.858	50527.998	03/20/97	5.0	6299	c
30	50531.703	50531.799	03/24/97	5.0	6001	c
31	50542.650	50542.715	04/04/97	4.0	3157	c
32	50548.520	50548.577	04/10/97	5.0	2841	c
33	50554.770	50554.917	04/16/97	5.0	8577	c
34	50562.797	50562.821	04/24/97	5.0	1536	c
35	50568.581	50568.657	04/30/97	5.0	3642	c
36	50576.462	50576.549	05/08/97	4.3	4092	c
37	50580.650	50580.738	05/12/97	5.0	5292	c
38	50588.353	50588.458	05/20/97	5.0	4594	c
39	50596.319	50596.424	05/28/97	4.0	6919	c
40	50604.268	50604.363	06/05/97	5.0	5647	c
41	50608.401	50608.572	06/09/97	5.0	5965	c
42	50618.339	50618.365	06/19/97	5.0	2187	c
43	50625.825	50625.879	06/26/97	5.0	2392	c
44	50633.482	50633.568	07/04/97	5.0	5129	c
45	50637.480	50637.649	07/08/97	5.0	8993	c
46	50643.211	50643.489	07/14/97	5.0	7204	c
47	50653.504	50653.638	07/24/97	5.0	6047	c
48	50658.351	50658.422	07/29/97	5.0	3918	c
49	50663.664	50663.672	08/03/97	3.0	630	c
50	50674.438	50674.473	08/14/97	5.0	2973	c
51	50678.566	50678.607	08/18/97	5.0	3511	c
52	50685.434	50685.475	08/25/97	4.0	3504	c

[a] Noninteger values are given when a PCU was operated for a fraction of the observation.

[b] PCA EA modes are coded as follows: a (B_4MS_8A_0_49_H E_1US_4A_50_8S), b (B_2MS_4B_0_35_H E_16US_16B_36_1S SB_62US_0_35_500MS), and c (SB_125US_0_13_1S SB_125US_14_23_1S SB_125US_24_35_1S E_16US_16B_36_1S).

relatively narrow profiles. These changes in the power spectra coincide with the episode of spectral hardening seen in the ASM (see Fig. 1). Further spectral analysis of this low, hard state is deferred to a later publication.

To derive the central frequencies and widths of each QPO, we fitted the power spectra to a local continuum, using a power-law function, plus a QPO assumed to have a Lorentzian profile. We used a least-squares technique to determine the best fit. In the range of 7–28 Hz, we allowed for the presence of two overlapping QPOs with different widths. In order to maintain χ^2_ν values in the range 0.9–1.2, the locations of the fitting regions had to be adjusted for each observation, and on a few occasions we were forced to add a second broadband component when the QPO was

TABLE 2

PCA Count Rates and QPO Detections

Observations (1)	UT Date (2)	PCA Rate[a] (3)	σ (1 s bins) (4)	PCA (HR1)[b] (5)	PCA (HR2)[c] (6)	Soft (2–5 keV) (7)	Hard (9–25 keV) (8)	QPOs and Comments (9)
1.....	05/09/96	3556	156.8	0.417	0.075	2473	84	...
2.....	05/10/96	3724	130.8	0.413	0.075	2540	85	...
3.....	05/11/96	3649	133.5	0.416	0.075	2502	85	...
4.....	05/12/96	3671	157.2	0.422	0.076	2490	88	...
5.....	07/25/96	4721	289.6	0.468	0.155	2971	295	9.1, 20.1
6.....	08/01/96	7139	973.7	0.680	0.284	3511	1006	0.09, 8.7, 14.5, 277 (9)
7.....	08/06/96	6013	328.4	0.594	0.236	3307	657	11.1, 16.0, 306 (9)
8.....	08/15/96	4327	343.8	0.476	0.157	2719	280	9.4, 21.4
9.....	08/16/96	5165	252.4	0.524	0.224	3004	514	7.3, 16.8, 287 (9)
10	08/22/96	4937	305.5	0.501	0.198	2977	417	9.0, 17.9, 294 (8)
11	08/29/96	6820	246.1	0.639	0.265	3547	875	9.7, 14.7, 287 (11)
12	09/04/96	4727	337.5	0.471	0.167	2948	322	9.3, 18.7
13	09/09/96	4734	313.8	0.483	0.174	2921	341	9.5, 18.8
14	09/20/96	4119	245.0	0.452	0.147	2632	241	20.6
15	09/26/96	3854	293.9	0.432	0.106	2554	149	...
16	10/03/96	3806	281.6	0.447	0.121	2521	180	...
17	10/15/96	4595	383.3	0.481	0.142	2884	266	21.1
18	10/22/96	4766	412.9	0.469	0.147	3026	282	22.4
19	10/27/96	5775	411.2	0.531	0.197	3377	497	8.5, 17.7, 309 (14)?
20	11/02/96A	4328	354.5	0.609	0.299	2257	632	10.3
21	11/02/96B	6350	457.0	0.658	0.294	3209	935	0.10, 9.1
22	01/05/97	1754	183.3	0.352	0.127	1220	82	Dips
23	01/12/97	1589	47.6	0.308	0.093	1160	48	...
24	01/20/97	890	21.6	0.228	0.040	708	8	...
25	01/26/97	1123	28.3	0.259	0.070	856	22	...
26	02/26/97	2263	239.3	0.333	0.049	1650	30	Dips
27	03/05/97	2533	89.0	0.343	0.056	1831	40	...
28	03/10/97	2574	97.5	0.367	0.063	1836	50	...
29	03/20/97	2671	107.0	0.359	0.071	1863	60	...
30	03/24/97	2398	84.3	0.340	0.051	1736	33	...
31	04/04/97	2671	105.7	0.356	0.071	1891	59	...
32	04/10/97	2715	107.1	0.361	0.075	1915	65	...
33	04/16/97	2538	67.3	0.345	0.053	1833	36	...
34	04/24/97	2583	68.5	0.366	0.056	1860	41	...
35	04/30/97	2649	78.3	0.356	0.055	1898	40	...
36	05/08/97	2874	89.1	0.389	0.062	2022	53	...
37	05/12/97	2884	89.4	0.372	0.061	2022	49	...
38	05/20/97	3154	128.1	0.386	0.068	2205	65	...
39	05/28/97	3342	174.4	0.416	0.084	2217	94	...
40	06/05/97	3030	146.1	0.377	0.069	2128	63	...
41	06/09/97	2872	105.0	0.366	0.062	1996	51	...
42	06/19/97	2599	154.2	0.360	0.075	1823	63	...
43	06/26/97	2099	174.4	0.321	0.048	1584	27	...
44	07/04/97	1824	65.1	0.302	0.051	1356	25	...
45	07/08/97	1818	62.7	0.317	0.075	1324	43	...
46	07/14/97	1674	55.4	0.289	0.052	1256	23	...
47	07/24/97	1149	29.3	0.268	0.087	864	30	...
48	07/29/97	811	25.6	0.253	0.121	609	31	...
49	08/03/97	463	14.2	0.210	0.109	358	13	...
50	08/14/97	213	13.5	0.748	0.392	95	47	1.4, 6.4
51	08/18/97	61	8.4	0.945	0.475	23	18	0.2, 0.8
52	08/25/97	3.5	...	0.693	0.411	1.8	0.5	...

[a] PCA source rate at full bandwidth (effectively 2–25 keV) in units of counts s^{-1} PCU^{-1}.
[b] Ratio of 5–9 and 2–5 keV source count rates.
[c] Ratio of 9–13 and 5–9 keV count rates.

located near a break in the power continuum (see panel 11/02/96A in Fig. 2). The central QPO frequencies derived from these fits are included in Table 2, while all of the QPO parameters for individual detections in the range of 0.1–28 Hz are given in Table 3. These parameters include the central frequency (ν), the width ($\Delta\nu$; FWHM), the coherence parameter ($Q = \nu/\Delta\nu$), and the QPO amplitude, which is the integrated power normalized to the mean count rate of GRO J1655−40 in the appropriate energy band. The strongest QPO, during observation 11/02/96A, has an amplitude of $4.5\% \pm 0.6\%$ (2–25 keV) centered at 10.3 ± 0.2 Hz with $\Delta\nu = 2.2 \pm 0.3$ Hz. The weakest QPOs,

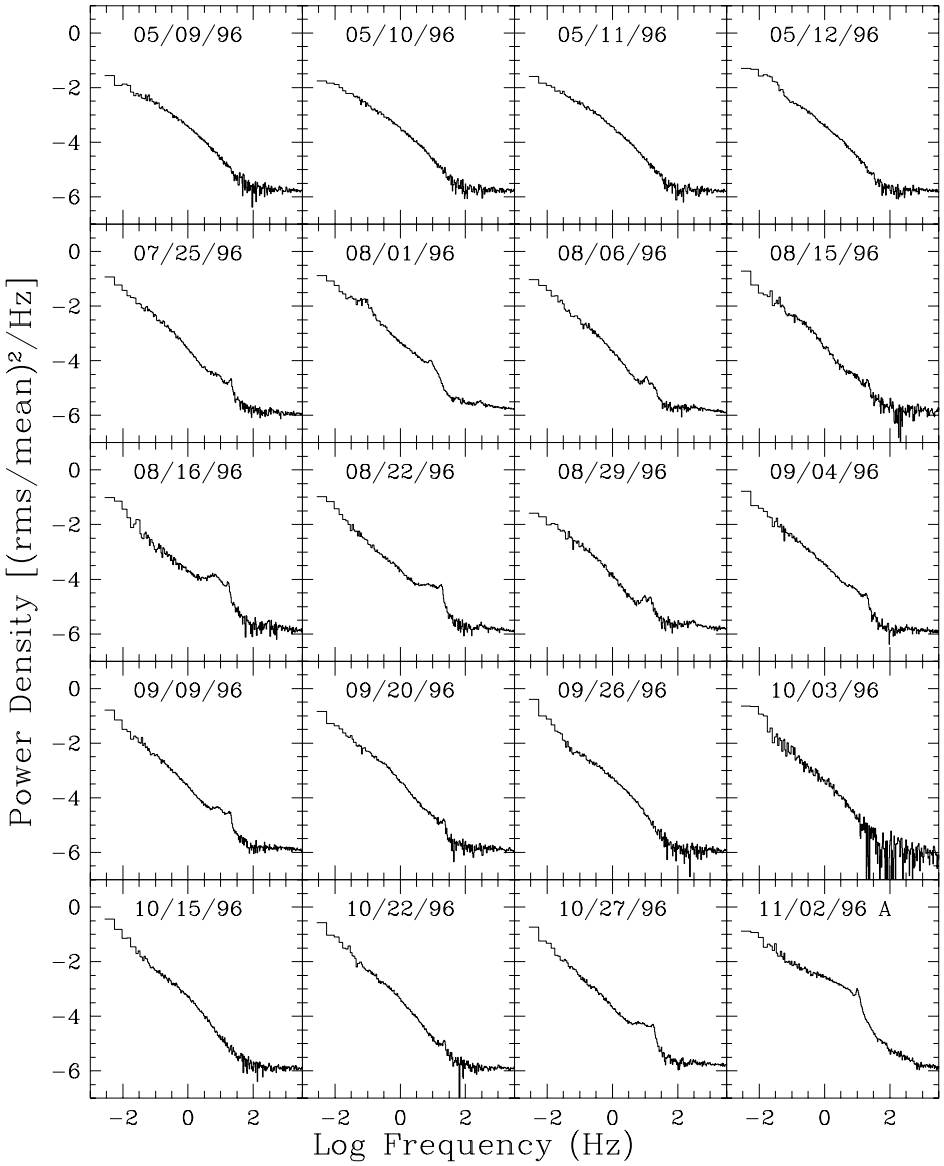

FIG. 2.—PCA power spectra of GRO J1655−40 for the first 20 observations listed in Tables 1 and 2. The observation dates are given as mm/dd/yy. The Poisson noise level, corrected for instrument dead time, has been subtracted.

with amplitudes ∼0.5%, have typical uncertainties (1 σ) of 0.1% in amplitude, 0.3 Hz in ν, and 0.4 Hz in $\Delta\nu$. We will show that the broadest of these features ($1 < Q < 3$) exhibit spectral properties and occurrence patterns that are generally different from the more narrow features ($Q > 3$) that resemble the QPOs seen in other sources (van der Klis 1995).

The X-ray source properties summarized in Table 2 can be used to predict the presence of QPOs at 7–28 Hz. Excluding the low/hard state at the end of the 1996–1997 outburst, the approximate thresholds for QPO activity are a 2–25 keV count rate of 4000 counts s^{-1} PCU^{-1}, a 9–25 keV count rate of 200 counts s^{-1} PCU^{-1}, a value of 0.45 in PCA HR1 (counts at 5–9 keV relative to 2–5 keV), or a value of 0.14 in PCA HR2 (counts at 9–13 keV relative to 5–9 keV). These thresholds are all related to the appearance of substantial flux above 9 keV, which suggests that the QPO mechanism is linked to the source of relativistic electrons that are believed to radiate the hard X-ray component. In the case of GRS 1915+105, the increase in QPO amplitudes with photon energy supported a similar conclusion (Morgan et al. 1997). Further considerations regarding the spectral characteristics of the 0.1–28 Hz QPOs are given below.

3.2. *Detection of a QPO at* 300 Hz

The relationship between QPO activity and the hard X-ray spectrum motivated us to combine the individual power spectra in groups determined by their spectral hardness, in order to search for more subtle features, especially at higher frequency. Using the PCA HR1 values given in Table 2, we sorted and combined the individual power spectra (excluding observations 50–52) into four groups: 1996 and HR1 < 0.45 and 1997 and HR1 < 0.45, 0.45 < HR1 < 0.50, and HR1 > 0.50. We label these groups, respectively, "soft 1996," "soft 1997," "hard," and "very hard." For each group, we computed weighted averages for each frequency bin, again using photon detections over 2–25 keV. The results are shown in Figure 5, where four important details can be noted: (1) The 27 power

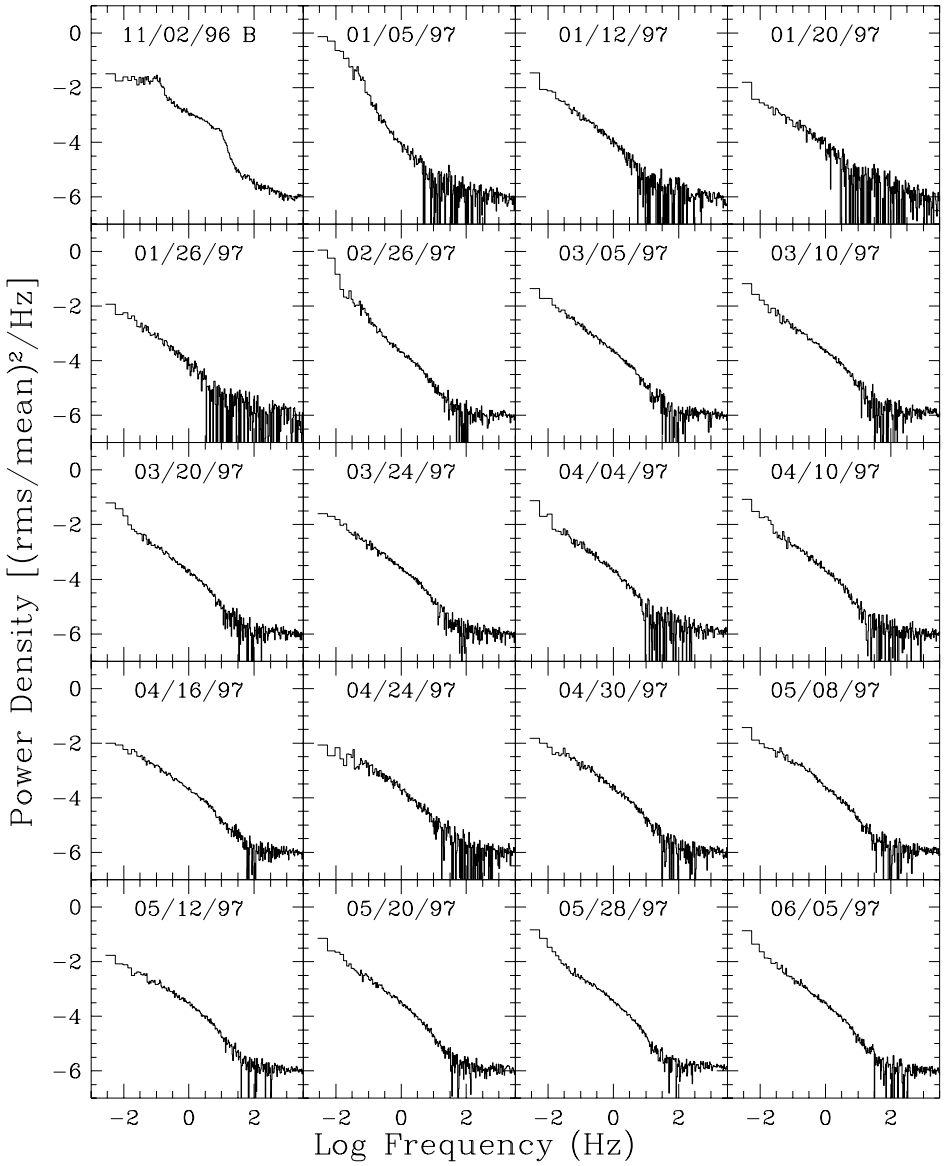

FIG. 3.—Same as Fig. 2, but for the subsequent 20 observations

spectra in the group soft 1997 do provide a narrow QPO just below 30 Hz. (2) There is a suggestion that the QPOs move to lower frequency as the spectrum becomes harder. (3) The QPO near 0.1 Hz is apparent in the very hard group. (4) Finally and most importantly, there is a broad bump near 300 Hz for the very hard group.

In Figure 6 we replot Figure 5 with a magnified scale to provide closer inspection of those QPO features above 10 Hz. We fitted the profiles for two of the QPOs, as described above. The QPO for the soft 1997 group is located at 27.5 ± 0.8 Hz with $\Delta\nu = 3.1 \pm 1.5$ Hz and an amplitude of $0.35\% \pm 0.10\%$ over 2–25 keV. The χ^2_ν value for the fit is 0.9. In the remainder of § 3.2 we focus solely on the broad feature near 300 Hz.

The QPO fit at 300 Hz for the very hard group (Fig. 6) yields a central frequency of 295 ± 9 Hz, a FWHM of 73 ± 15 Hz, and an integrated amplitude of $0.81\% \pm 0.11\%$. The significance of this QPO detection is therefore above 7 σ.

The origin of the 300 Hz feature within the very hard group is investigated in Figure 7. Here the A and B observations of 1996 November 2 have been combined. The fit for the local power continuum is shown with a solid line. A weak power excess near 300 Hz is seen in the first five or six of these seven observations. We conclude that the 300 Hz feature is statistically diluted among the individual power spectra, as would be expected for observations of a very weak yet stationary process.

If we select only the 1996 August observations within the very hard group (i.e., Fig. 7, *top five panels*) and refit the continuum and QPO profile, then the detection significance is again above 7 σ, with $\nu = 290 \pm 8$ Hz and $\Delta\nu = 67 \pm 14$, and the amplitude is $0.85\% \pm 0.12\%$.

The upper limit (90% confidence) for a QPO in the range of 250–350 Hz (with $\Delta\nu = 70$ Hz) is 0.40% of the mean flux for the hard group, 0.17% for the soft 1997 group, and 0.43% for the soft 1996 group. We therefore conclude that the 295 Hz QPO in GRO J1655−40 is significantly weaker

TABLE 3

QPO Fit Parameters

Observation	Date	ν	$\Delta\nu$	Q	Amplitude
5	07/25/96	9.1	5.4	1.7	0.0095
5	07/25/96	20.1	5.4	3.7	0.0110
6	08/01/96	0.086	0.058	1.5	0.0287
6	08/01/96	8.7	4.1	2.1	0.0189
6	08/01/96	14.5	4.5	3.2	0.0090
7	08/06/96	11.1	1.5	7.3	0.0054
7	08/06/96	16.0	10.5	1.5	0.0123
8	08/15/96	9.4	5.0	1.9	0.0084
8	08/15/96	21.4	4.7	4.6	0.0078
9	08/16/96	7.3	7.2	1.0	0.0332
9	08/16/96	16.8	2.5	6.7	0.0132
10	08/22/96	9.0	8.3	1.1	0.0225
10	08/22/96	17.9	3.5	5.1	0.0173
11	08/29/96	9.7	3.4	2.9	0.0081
11	08/29/96	14.7	3.1	4.7	0.0078
12	09/04/96	9.3	7.0	1.3	0.0146
12	09/04/96	18.7	4.5	4.2	0.0127
13	09/09/96	9.5	7.4	1.3	0.0154
13	09/09/96	18.8	4.7	4.0	0.0110
14	09/20/96	20.6	3.4	6.1	0.0076
17	10/15/96	21.1	2.2	9.6	0.0032
18	10/22/96	22.4	3.3	6.8	0.0058
19	10/27/96	8.5	7.0	1.2	0.0180
19	10/27/96	17.7	4.5	3.9	0.0151
20	11/02/96A	10.3	2.2	4.7	0.0454
21	11/02/96B	0.100	0.082	1.2	0.0442
21	11/02/96B	9.1	4.4	2.1	0.0279
22–48	soft 97	27.5	3.1	8.9	0.0035

or absent when the luminosity in the power-law component falls below that of the very hard group (i.e., when HR1 < 0.5).

Finally, the effort to ascertain whether the central frequency of this QPO has a constant value is limited to the weak indications provided in Figure 7. We searched for a QPO with a central frequency in the range of 250–350 Hz for each individual panel shown in Figure 7; the power spectra in the top six panels yield a sample of central frequencies that are distributed as 293 ± 12 Hz (see Table 2). The variations in frequency are consistent with the statistical limitations of these measurements, which have an rms uncertainty of 10.3 Hz in the QPO central frequency. Meanwhile, the count rates in the hard PCA band (i.e., above 9 keV) for these same six observations vary by a factor of 2.5 (max/min). Since the flux in hard photons is highly correlated with the appearance of this QPO and since the hard flux variations are much larger than the dispersion in central frequency, we regard these results as an indication of frequency stability in the 300 Hz feature.

3.3. *QPO Properties versus Photon Energy*

Our detection of the 300 Hz QPO in GRO J1655−40 is limited to just one energy channel (2–25 keV) for the following reason: The operating modes for the PCA event analyzers (EAs) are given in Table 1. During the very hard observations (1996 August–November), the four discretionary PCA EAs were operated in parallel in the following modes: (1) a four-channel binned mode with 2 ms time resolution at 2–13 keV; (2) a single-channel, "single bit" mode with 62 μs time resolution at 2–13 keV; and (3) a 16 μs event mode for photons above 13 keV. In order to detect a 295 Hz oscillation the data must be sampled with a time resolution finer than 1.7 ms, but the 2 ms data from the four-channel binned mode is inadequate for this task. We therefore have only two channels, divided at 13 keV, with which to examine phenomena at frequencies above 250 Hz. During the very hard observations, the 13–25 keV source count rate was only 10%–18% of the rate below 13 keV, and we do not detect a significant QPO in these data. The PCA time resolution was increased to four-channel cover-

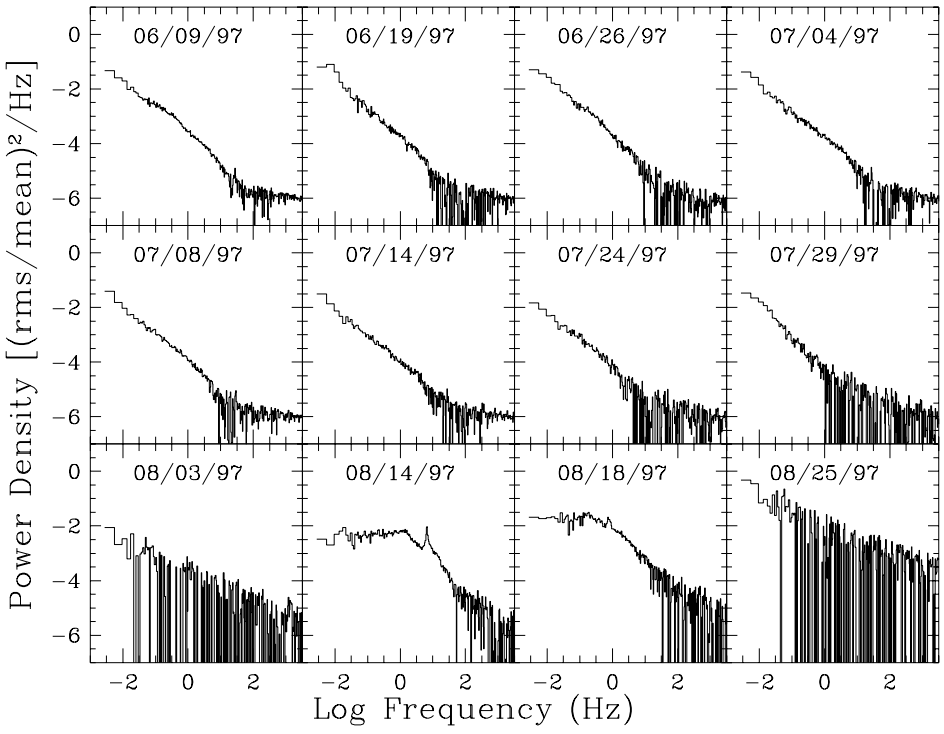

Fig. 4.—Same as Fig. 2, but for the last 12 *RXTE* observations

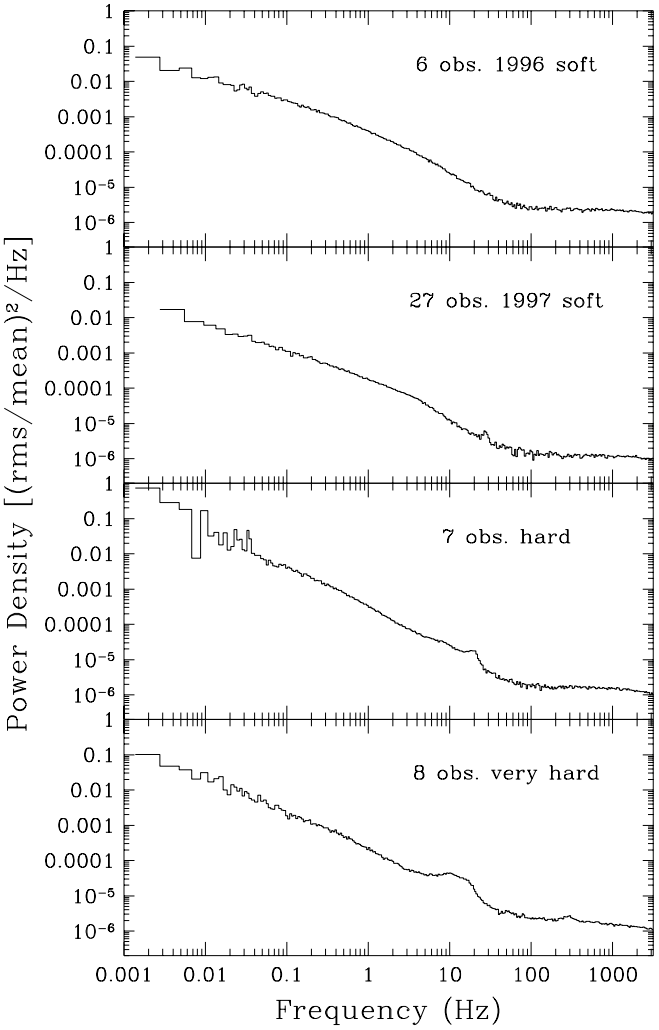

FIG. 5.—Combined power spectra of GRO J1655−40 in which the first 49 PCA observations are combined into four groups organized by intervals of PCA HR1 and the year of observations (see text).

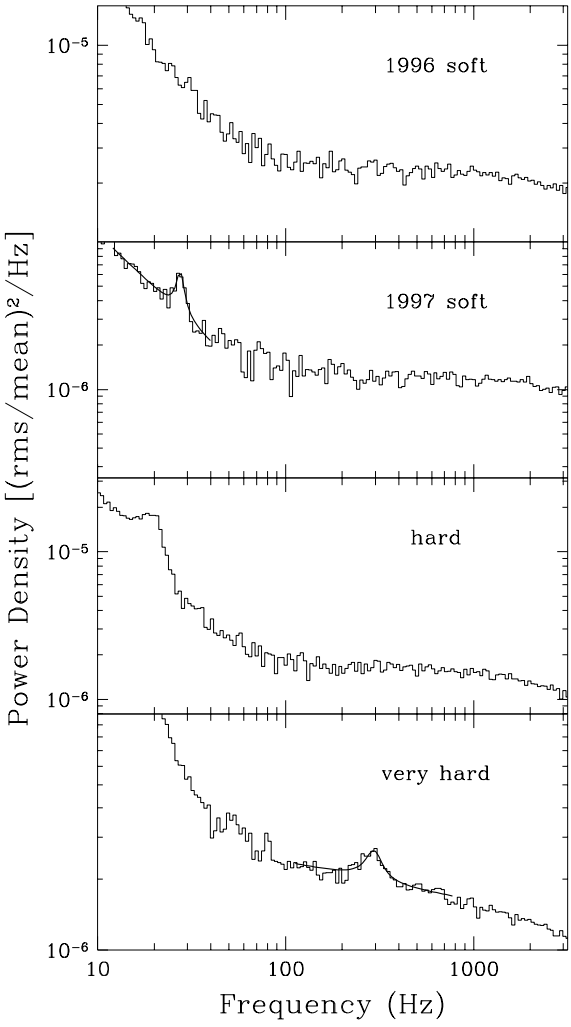

FIG. 6.—Magnified view of a portion of Fig. 5. A QPO appears at 300 Hz during the eight observations with the hardest X-ray spectra.

age with 125 μs time resolution for the 1997 observations, but there was no detection of the fast QPO during this period.

For the low-frequency QPOs, however, we can easily measure the QPO properties for hard and very hard observations in five different energy bands, with four bands telemetered in binned mode and the highest energy band obtained from event mode. We show two energy-resolved series of power spectra in Figure 8. The left panels show results for an observation in the very hard group (08/16/96), while the right panels show results for an observation in the hard group (09/09/96). Both cases show a broad QPO near 8–10 Hz combined with a narrower QPO at higher frequency. The central frequencies for the two-QPO fits (2–25 keV) for each observation are shown with arrows in the top and bottom panels. The energy-resolved power spectra in Figure 8 show that the broad and narrow QPOs have very different energy dependence: in both observations, the broad QPO is stronger at lower photon energies, while the narrow QPO shows an increase in amplitude at higher photon energies.

Further insight into the broad-soft and narrow-hard QPOs are gained by plotting the central frequencies for the two-QPO fits versus the PCA count rate in the hard band (9–25 keV). The results are shown in Figure 9. The plotting symbols distinguish broad and narrow QPOs using the coherence parameter, Q, as defined previously. The asterisk indicates broad QPOs with $Q < 3.0$, while the open triangles denote narrow QPOs with $Q > 3.0$. The data point marked with the "X" represents the narrow and weak QPO for the entire soft 1997 group, as shown in Figure 6. This 28 Hz QPO appears to be a simple extrapolation of the narrow QPO branch shown in Figure 9. The frequency of narrow QPOs is correlated with the intensity in hard X-rays, shifting from 28 to 14 Hz as the hard intensity increases from zero to maximum. This is the only QPO that is visible as the count rate at 9–25 keV approaches zero. On the other hand, the broad QPOs near 9 Hz in Figure 9 remain essentially stationary, and this QPO is not observed when the soft component dominates the spectrum. There are some exceptions to the pattern of QPO branches in Figure 9. For example, we do not detect two distinct QPOs for every observation in the hard groups, and two of the QPO detections near 9 Hz appear to be relatively narrow in FWHM. Nevertheless, the weight of the evidence suggests that there are two quite different and yet coexisting types of QPOs in GRO J1655−40 in the range of 7–28 Hz.

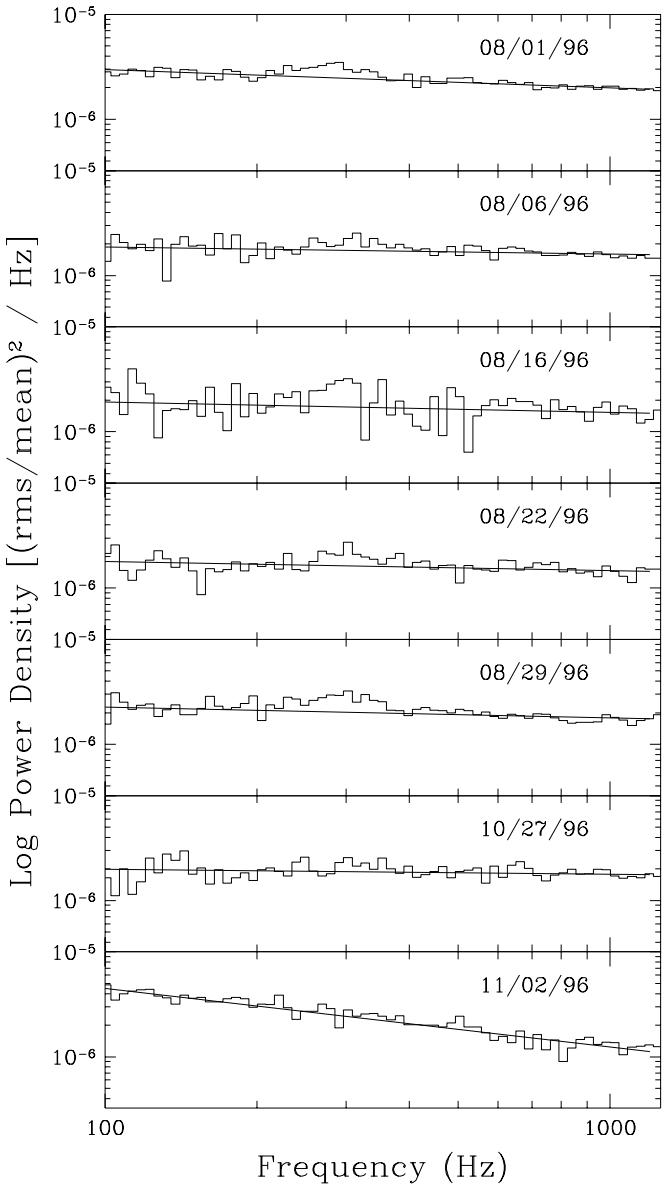

FIG. 7.—Power spectra in the very hard group shown individually (*histograms*) along with the fit to the local power continuum (*solid line*). In this figure, the A and B observations of 11/02/96 have been combined. The 300 Hz QPO appears weakly visible in the upper five or six panels, as would be expected from statistical effects when observing a stationary process.

3.4. *QPOs at* 0.1 Hz *and a Connection to GRS* 1915+105

The power spectra of 08/01/96 (Fig. 2) and 11/02/96B (Fig. 3) each display a low-frequency QPO near 0.1 Hz. These same two observations are at the extreme end of the very hard group, yielding the highest values for the X-ray intensity at 9–25 keV, as shown in Table 2 and Figure 9. The 0.1 Hz QPOs lie atop substantial broadband power, and their integrated rms power values (2.9% and 4.4% of the mean count rate, respectively) rank them among the QPOs in GRO J1655−40 with the highest amplitudes (see Table 3) but with the lowest coherence ($Q < 2$).

The appearance of low-frequency QPOs during conditions of high X-ray luminosity in GRO J1655−40 is reminiscent of the behavior of the microquasar GRS 1915+105. The latter source is prone to episodes of tremendous X-ray variability (Greiner, Morgan, & Remillard 1996), but there are also occasions when the X-ray intensity of GRS 1915+105 is relatively low and steady, and there are other occasions characterized by intermediate brightness, moderate flickering, and QPOs near 0.1 Hz (Morgan et al. 1997). In particular, the power spectra of GRS 1915+105 on 1996 April 17–May 14, 1996 September 22, 1997 August 13, and 1997 November 7–30 show QPOs near 0.1 Hz. The corresponding light curves show substantial flickering, but there are no large cyclical variations, and the rms deviation (1 s bins) is less than 30% of the mean value.

There is an especially striking resemblance between the PCA observation of GRO J1655−40 on 1996 August 1 and the observation of GRS 1915+105 on 1997 August 13. In each case, the source appears to shift back and forth between a state of relatively steady emission and another condition in which both the intensity and the hardness ratio are strongly modulated by a 0.1 Hz QPO. This behavior is illustrated for both sources in Figure 10. Both the X-ray intensity and the variability of GRO J1655−40 are as large as we have seen with *RXTE*. However, GRS 1915+105 has shown a wide variety of much deeper oscillations on timescales ranging from seconds to ~30 minutes. Given the similarities shown here and the extraordinary behavior observed for GRS 1915+105 (Greiner et al. 1996), one may speculate that GRO J1655−40 is on the verge of plunging into unstable X-ray emission on 1996 August 1. Figure 10 displays the closest link we have seen between GRO J1655−40 during its radio-quiet X-ray outburst of 1996–1997 and GRS 1915+105, which has been wildly active at both X-ray and radio frequencies (Fender et al. 1997; Pooley & Fender 1997; Eikenberry et al. 1998; Mirabel et al. 1998). In § 5 we use these intermittent 0.1 Hz QPOs, combined with spectral analyses and our knowledge of the black hole mass in GRO J1655−40, to speculate on the mass of the black hole in GRS 1915+105.

4. X-RAY SPECTRAL ANALYSIS BY QPO GROUP

Thus far we have described several relationships between QPO characteristics and the X-ray spectrum by correlating the QPO parameters with PCA count rates and hardness ratios. In these interpretations we have assumed that the X-ray spectrum of GRO J1655−40 can be described by a standard model consisting of a thermal component and a hard power law, with a minimal contribution from the thermal component above 9 keV. Zhang et al. (1997) used *ASCA* and BATSE observations of GRO J1655−40 during 1995 August 15–16 to show that this spectral model produced an acceptable fit with an inner disk temperature of 1.36 keV. A detailed spectral analysis of observations discussed herein, and the systematic problems regarding physical interpretations of the fit parameters, is given by Sobczak et al. (1999). For the purposes of the present paper, we have investigated the mean spectra for each QPO-sorted group (§ 3.2). The results confirm our conclusions that QPO activity in GRO J1655−40 is strongly linked to the strength of the power-law component.

We used XSPEC to analyze these data, assuming a multitemperature "disk-blackbody" model plus a power-law function, both attenuated by absorption due to cold gas along the line of sight. The analysis was performed with the 1998 January 20 version of the PCA spectral response matrices. Since the high count rates and long exposure times for GRO J1655−40 stringently test the quality of the

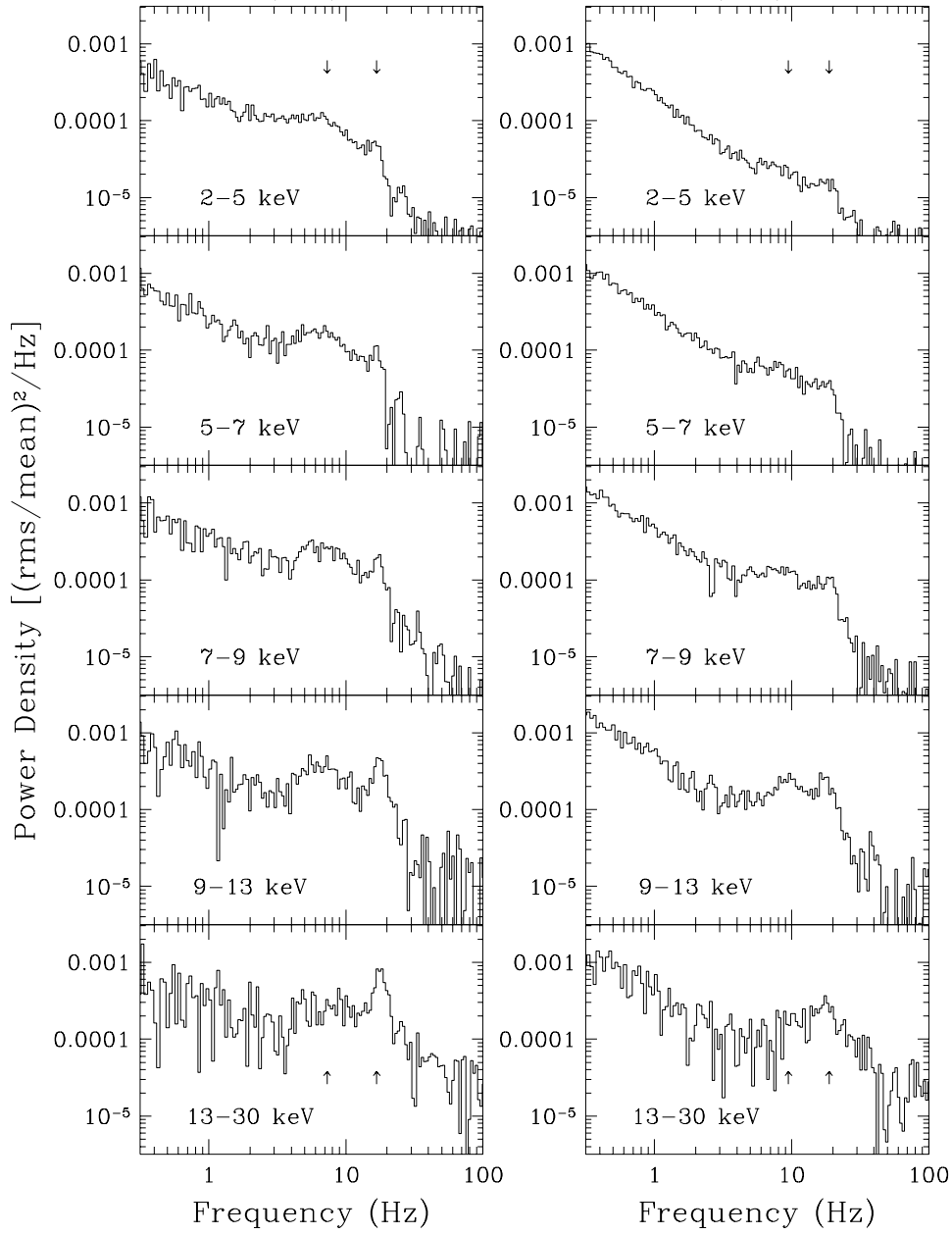

FIG. 8.—Energy-resolved power spectra of two observations among those that appear to have both broad and narrow QPOs. The left panels show results for an observation (9) in the very hard group (8/16/96), while the right panels show results for an observation (13) in the hard group (09/09/96). There appears to be a broad and relatively soft QPO near 8–10 Hz combined with a more narrow and hard QPO at higher frequency. The central frequencies for the two-QPO fits for each observation are shown with arrows in the top and bottom panels.

PCA spectral calibrations, we first investigated the spectra derived from long exposures of the Crab Nebula on 1997 March 22, April 15, and July 26. Systematic features in the fit residuals are most evident in PCUs 2 and 3. We have concluded that the best performance from these particular response matrices is gained by choosing PCUs 0, 1, and 4 (only), by restricting the analysis range to 2.5–25.0 keV (with 54 data channels from PCA standard mode 2), and by imposing a systematic error of 1.0% on each data point. The statistical error bars for the spectral parameters in each group are very small, and so we conservatively choose to analyze independently the spectra provided by each of the three PCUs, and then we use the sample standard deviation as the uncertainty in each spectral parameter. The absolute normalizations of PCU 4 are chronically 10% lower than those of PCUs 0 and 1, and we accordingly raised the normalizations for PCU 4 before reporting the results. Finally, all of the spectral results (unlike the counting rates reported in Table 2) include considerations of the PCA dead time, with correction factors ranging from 1.047 to 1.109 for the data groups associated with Table 4.

We conducted spectral fits in which we considered the value of the interstellar column density (N_H) as a free parameter, and then we repeated the analysis with $N_H = 0.9 \times 10^{22}$ cm^{-2}, which is the value found with *ASCA* (Zhang et al. 1997). The results for both cases are shown in Table 4. Although the fitted versus fixed values of N_H are statistically different in most cases, this difference has only a minor effect on the other spectral parameters or the integrated flux.

The reduced χ^2_ν values (Table 4) for these spectral fits are

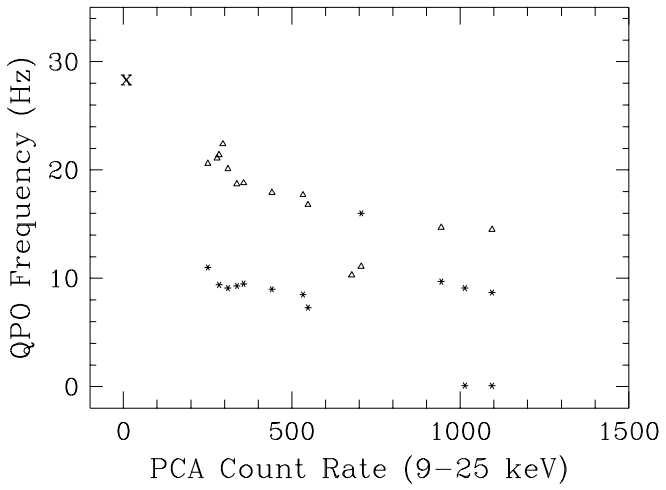

FIG. 9.—QPO frequency vs. the PCA count rate in the hard band (9–25 keV). The results are determined from two-QPO fits to the power spectra for the range of 6–35 Hz. The asterisk is used for broad QPOs, in which $Q < 3.0$, while the open triangles denote narrow QPOs with $Q > 3.0$ (see text). The data point plotted with the "X" represents the weak QPO and the mean hard count rate from the entire soft 1997 group (see Fig. 6).

reasonably good for the hard and very hard groups, with total exposure times ~ 40 ks PCU^{-1} for each group. On the other hand, the soft spectra, and particularly the soft 1996 (58 ks) group, were not well fitted with the disk-blackbody plus power-law model. We modified the model with the addition of Fe emission lines, absorption edges, and Compton reflection, but the fits remained unacceptable. The separation of the soft 1996 group into subsections A (1996 May 9–12) and B (September 26 and October 3) temporally isolated this unsolved problem. During the 1996 May observations, which occurred 14–17 days after the beginning of the X-ray outburst, we find $\chi^2_\nu \sim 20$ for the disk-blackbody and power-law model. However, the fit is quite satisfactory ($\chi^2_\nu = 1.04$) for the "soft 1996B" group. Model problems are again encountered for the soft 1997 group (102 ks exposures per PCU). However, the residuals are only $\sim 2\%$ of the net flux, and we argue that the comparison of spectral parameters with the other groups provides useful information, despite the elevated value of χ^2_ν. We further investigated the soft states with an alternative model consisting of a disk blackbody combined with an exponential function, as successfully used for particular soft states in GRS 1915+105 (Muno, Morgan, & Remillard 1999). The fit was significantly improved but formally unacceptable ($\chi^2_\nu \sim 8$ for the "soft 1996A" spectrum). The fit parameters for this alternative model are included in Table 4. The fit improvement for an exponential hard tail, rather than a power law, may suggest a saturated form of Comptonization in which a modest supply of energetic electrons is efficiently cooled by collisions with ambient photons.

The fit parameters and the deduced unabsorbed fluxes and luminosities for the various spectral groups are given in Table 4. The results exhibit patterns of X-ray spectral evolution in GRO J1655−40. As the total luminosity increases, the disk color temperature increases from ~ 1.1 to nearly 1.5 keV, while the normalization decreases by a factor of 5. This behavior is confirmed in a more detailed spectral analysis of the same observations by Sobczak et al (1999), which includes HEXTE observations. In terms of energy flux from the thermal component, the drop in the disk normalization is more significant than the increase in temperature. The total luminosity slowly rises from the soft states to the very hard state, while there is a large change in the relative contribution of the two components. The thermal component contributes $\sim 90\%$ of the 1–25 keV unabsorbed flux during the soft states. The flux in the power-law component rises sharply as the spectrum hardens, as we had deduced from the PCA hardness ratios. In the hard group, the power-law component represents $\sim 27\%$ of the unabsorbed X-ray flux (1–25 keV), and this fraction increases to $\sim 75\%$ in the very hard group. In both the hard and very hard groups, the photon index is in the range of 2.4–2.7, which is very similar to the results obtained in earlier outbursts for the range of 20–600 keV with the *Compton Gamma-Ray Observatory* (*CGRO*; Kroeger et al. 1996; Zhang et al. 1997). The 1996 August 29 PCA observation was combined with *RXTE* HEXTE and *CGRO* OSSE observations to measure a photon index of 2.7 with a lower limit of 800 keV for the cutoff energy associated with the power-law component (Tomsick et al. 1999). Here we obtain a similar value (2.62) in the photon index for the very hard group, which indicates that the power-law component is well determined despite the 25 keV limit in our spectral fits.

Our spectral results allow us to estimate the thresholds for QPO activity in terms of $L_{\rm Edd}$, which is 8.4×10^{38} ergs s^{-1} for a 6.7 $M_\odot$ black hole. We note that the conversion of unabsorbed flux to luminosity involves only the factor of $4\pi d^2$ for the power-law component, but a factor of $2\pi d^2/\cos(69^\circ.5)$ for the disk blackbody.

The threshold where the broad 9 Hz QPO appears is $L_{\rm X} \sim 0.1 L_{\rm Edd}$. We detect 300 Hz QPOs above $L_{\rm X} \gtrsim 0.2 L_{\rm Edd}$, and 0.1 Hz QPOs appear at a slightly higher value, $L_{\rm X} \sim 0.25 L_{\rm Edd}$. Perhaps more significantly, the QPOs at 300 and 0.1 Hz are only seen when the power-law component is the dominant source of X-ray luminosity.

5. DISCUSSION

The 300 Hz QPO in GRO J1655−40 is the fastest oscillation ever seen in a black hole binary. Efforts to explain this feature and also the 67 Hz QPO in GRS 1915+105 commonly invoke effects of GR, and these results provide an important opportunity to investigate the properties of these black holes via the physics of strong gravitational fields (see McClintock 1998). There are at least six physical timescales of the inner accretion disk in a black hole binary that have been discussed in the context of fast QPOs at X-ray energies. These are the last stable orbit (Shapiro & Teukolsky 1983; Morgan et al. 1997), diskoseismic oscillations (Wagoner 1998; Perez et al. 1997; Nowak et al. 1997), frame-dragging (Merloni et al. 1999; Cui, Zhang, & Chen 1998), inertial-acoustic instabilities (Chen & Taam 1995), oscillations related to a centrifugal-barrier model (Titarchuk, Lapidus, & Muslimov 1998), and radial oscillations in the position of radiative shocks (Molteni, Sponholz, & Chakrabarti 1996). The physics of all of these phenomena invokes GR effects in the inner accretion disk.

Any model for the high-frequency QPOs in microquasars must also explain the observed amplitudes and spectral characteristics of these QPOs and the manner in which these properties vary with the state of the X-ray source. In the case of GRO J1655−40, the 300 Hz QPO is detected only in the very hard group, when the X-ray luminosity is above $0.2 L_{\rm Edd}$ and the power-law component dominates the

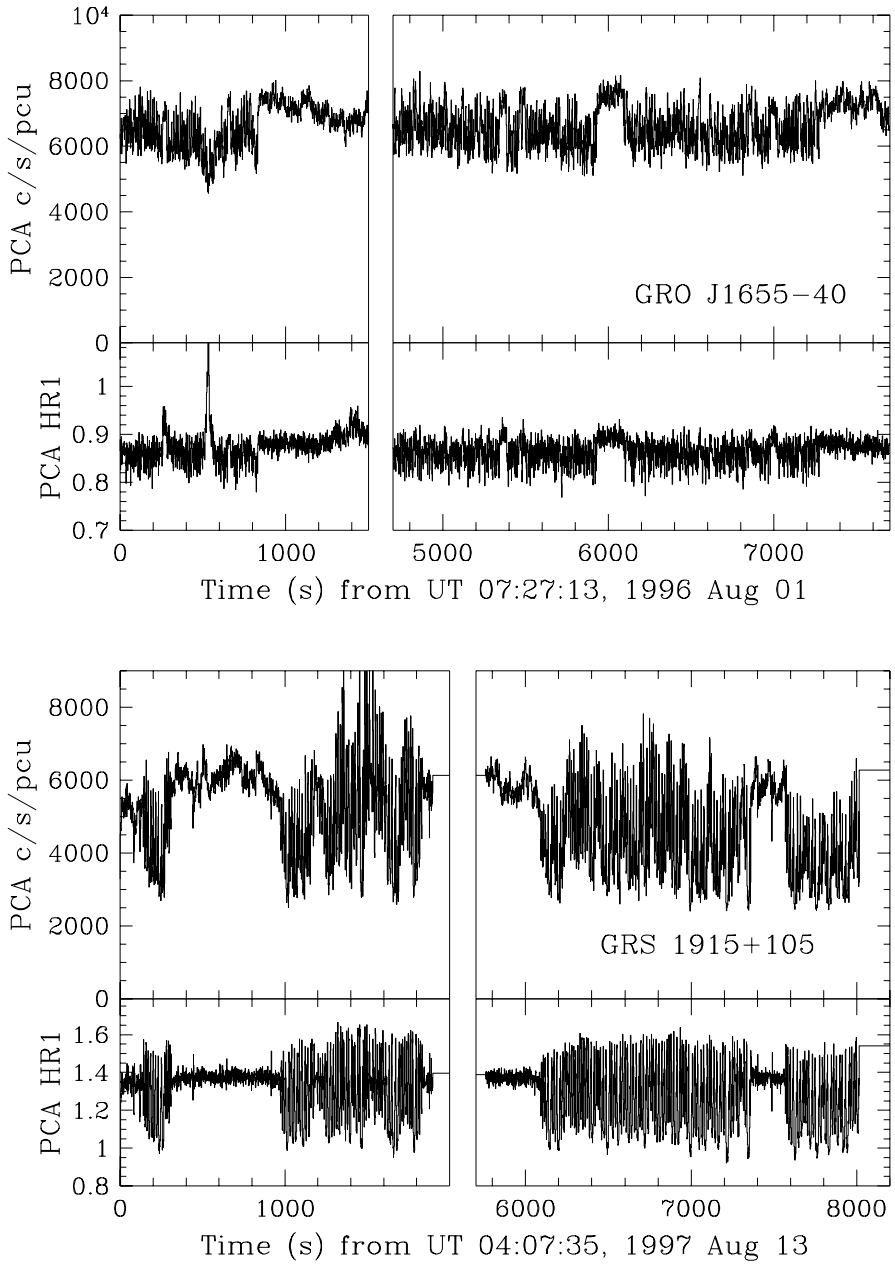

FIG. 10.—PCA observation of GRO J1655−40 on 1996 August 1 (*top panels*) showing the light curve (2–25 keV) and the values of the hardness ratio, PCA HR1. Very similar results were obtained during a PCA observation of GRS 1915+105 on 1997 August 13 (*lower panels*). In both cases, the X-ray emission teeters between a relatively steady emission state and another state with rapid oscillations at 0.1 Hz.

spectrum. The upper limits for 300 Hz QPOs in the other groups imply that this QPO is at least a factor of 2–3 weaker (in percent amplitude) in fainter states, when the disk emission dominates the spectrum. Therefore, the effort to explain the fast QPO in terms of variability timescales in the inner disk must confront the physical origin of the power-law component, which remains unknown. Since we measure the QPO amplitude as a percentage of detected source counts, we note that the deconvolution of the spectral components in terms of PCA detected count rates indicates that 33% of the PCA counts (full bandwidth) in the very hard state come from the disk, while 67% originate in the power-law component. The spectral constraints on the origin of the 67 Hz QPO in GRS 1915+105 are even more challenging for disk oscillation models, since the QPO amplitude has been shown to be as high as 6% at photon energies above 13 keV, where the disk contributes a small fraction of the X-ray flux (Morgan et al. 1997). The multiplicity of models and the incomplete connections between inner disk timescales and the spectral properties of the high-frequency QPOs remain as outstanding problems in this field.

Zhang et al. (1997) have outlined GR corrections to the disk-blackbody model that allow the estimation of the real temperature and radius of the inner accretion disk from the measured values of $T_{\rm col}$ and the disk-blackbody normalization. While there are uncertainties in the accuracy of the corrections for spectral hardening in the disk atmosphere (Shimura & Takahara 1995), the behavior of GRO J1655−40 should motivate further concerns about the

TABLE 4

X-RAY SPECTRAL PARAMETERS FOR GRO J1655−40[a]

Group	Number of Observation	χ^2_ν	N_H (10^{22} cm^{-2})	T_{col} (keV)	Disk Normalization	Power-Law Index	Hard Normalization	E_c (keV)	Flux[b] (Disk-blackbody)	Flux[b] (Hard)	L_X[c]
Soft 96a	4	19.86	2.21 (5)	1.24 (1)	1570 (38)	4.50 (9)	146.0 (56)	...	8.03	1.65[d]	1.60
Soft 96b.....	2	1.04	1.12 (4)	1.26 (2)	1615 (22)	2.22 (1)	2.40 (5)	...	8.81	0.89	1.65
Hard	7	0.70	0.62 (1)	1.30 (1)	1220 (33)	2.46 (2)	10.61 (24)	...	7.54	2.85	1.67
Very hard.....	8	1.27	1.51 (3)	1.43 (1)	418 (32)	2.67 (1)	51.9 (50)	...	3.78	10.97	2.00
Soft 97	27	4.19	1.88 (5)	1.10 (1)	2211 (31)	2.42 (3)	0.64 (7)	...	7.00	0.18	1.24
Soft 96a	4	24.01	0.90 (0)	1.26 (1)	1392 (29)	4.24 (9)	64.9 (20)	...	7.59	0.98[d]	1.45
Soft 96b.....	2	1.14	0.90 (0)	1.26 (2)	1570 (24)	2.20 (2)	2.23 (5)	...	8.56	0.85	1.59
Hard	8	0.84	0.90 (0)	1.29 (1)	1366 (28)	2.49 (1)	11.7 (3)	...	8.18	3.04	1.80
Very hard.....	7	1.77	0.90 (0)	1.49 (2)	376 (13)	2.62 (2)	47.5 (9)	...	4.01	10.61	2.00
Soft 97	27	6.71	0.90 (0)	1.12 (1)	1950 (21)	2.30 (3)	0.47 (4)	...	6.64	0.16	1.18
Soft 96a	4	7.79	0.90 (0)	1.18 (1)	2174 (21)	...	0.35 (5)	2.55 (8)	9.12	0.11	1.60
Soft 97	27	5.15	0.90 (0)	1.13 (1)	1880 (13)	...	0.006 (1)	7.89 (7)	6.64	0.06	1.17

[a] The spectral fits assume a multitemperature disk blackbody combined with a power-law component, except for the two cases at the bottom of the table where the power law was replaced with $\exp(h\nu/E_c)$, and the cutoff energy (E_c) is given instead of the photon index. The fits with N_H as a free parameter have 49 degrees of freedom. The uncertainties given in parentheses are in units of the most significant digit. The normalizations are corrected for PCA dead time, with a correction factor in the range of 1.047 (soft 97) to 1.109 (very hard).

[b] Values of the unabsorbed flux for the disk-blackbody and the hard X-ray component are given in units of 10^{-8} ergs cm^{-2} s^{-1} at 1–25 keV. Disk flux assumes an inclination of 69°.5

[c] The total unabsorbed luminosity is in units of 10^{38} ergs s^{-1} at 1–25 keV, for $i = 69°.5$ and $d = 3.2$ kpc.

[d] Flux at 2–25 keV only; the steep power spectrum overestimates the flux at low energy.

accuracy of inferring absolute conditions in the inner disk from the current tools in X-ray spectroscopy. The systematic increase in disk color temperature and decrease in the thermal normalization, as the flux in the power-law component increases, is not consistent with current disk theory (see Tanaka & Lewin 1995). The appearance of a small and hot inner disk may be due to spectral modifications imposed by a luminous Compton spectrum rather than the signature of an intrinsically small inner disk radius associated with a rapidly rotating black hole. The significant variations in disk color radius (or $f_{\rm DBB}\,T_{\rm col}^{-4}$) for GRO J1655−40 resemble the pattern of changes seen at much more rapid timescales (i.e., tens of seconds) in the case of GRS 1915+105 (Belloni et al. 1997b). However, in the present case there are no outward signs of disk instability, and throughout these observations GRO J1655−40 was in a radio quiet state.

While our analysis of QPO properties in GRO J1655−40 motivated a segregation of *RXTE* observations into groups defined by PCA hardness ratio, there is, in fact, a good correlation between these groups and the canonical states of black hole binaries (van der Klis 1994). The hard and very hard groups exhibit spectral properties and QPO behavior typical of the "very high state." This association extends the conclusions of Mendez, Belloni, & van der Klis (1998), that the microquasar GRO J1655−40 evolves through X-ray spectral states in a manner quite similar to other black hole binaries. Previous observations of X-ray sources in the very high state have been limited to transient conditions in GX 339-4 and GS 1124-68 (X-ray Nova Muscae 1991). There is also a suggestion that the chronic QPOs and high luminosity in GRS 1915+105 constitute some kind of variation of the very high state (Morgan et al. 1997). The QPO characteristics of GRO J1655−40 appear to bridge the phenomenology of GS 1124−68 and GRS 1915+105, and these *RXTE* results provide a large increase in the historical archive for the canonical form of the very high state.

To follow up on the similarity of particular *RXTE* observations of GRO J1655−40 and GRS 1915+105 presented in § 3.4 and Figure 10, we modeled the average spectrum for each observation as described in § 4. We then computed the luminosity, assuming a distances of 12.5 kpc and an inclination angle of 70° for GRS 1915+105. For GRO J1655−40 on 1996 August 1, we find that $T_{\rm col} = 1.71$ keV, the disk normalization is 194, the photon index is 2.50, and the power-law normalization is 48.5. The unabsorbed total luminosity is then 2.2×10^{38} ergs s^{-1} at 1–25 keV, or $L_{\rm X} \sim 0.26 L_{\rm Edd}$. Considering the power-law component only, $L_{\rm pl} \sim 0.18 L_{\rm Edd}$. In the case of GRS 1915+105 on 1997 August 13, we find $T_{\rm col} = 1.69$ keV, the disk-blackbody normalization is 340, the photon index is 3.17, and the power-law normalization is 90. The implied unabsorbed luminosity is then 3.88×10^{39} ergs s^{-1} at 1–25 keV, with 58% in the power-law component. If we speculate that the conditions in these two microquasars are similar with respect to the value of $L_{\rm Edd}$ in either the total luminosity or the power-law component, then GRS 1915+105 would harbor a massive black hole, with $M_1 \sim 100\,M_\odot$.

We have shown that the full composition of QPOs in GRO J1655−40 includes another quasi-stable frequency in the form of a broad QPO with 1%–3% amplitude at 9 Hz. This result complicates the application of the frame-dragging model to QPOs in black hole binaries (Cui et al. 1998). Here an 8 Hz QPO in GS 1124-68 was interpreted as being analogous to the 300 Hz QPO in GRO J1655−40. However, in this paper we have shown that there are two low-frequency QPOs in GRO J1655−40 that are much closer in frequency to the 8 Hz QPO in GS 1124-68, confusing the selection of QPOs that might represent the frame-dragging effect. Moreover, of the four QPO tracks in GRO J1655−40, only the 9 Hz QPO appears to have the soft X-ray spectrum expected for a purely disk-based oscillation. Clearly there is a need for additional opportunities to observe X-ray sources in the very high state, as we continue to investigate how to use X-ray QPOs to deduce the properties of black holes and also to determine the origin of the Compton electrons believed to radiate the hard X-ray spectrum.

This work was supported, in part, by NASA grant NAG 5-3680. Partial support for J. E. M. was provided by the Smithsonian Institution Scholarly Studies Program. C. D. B. acknowledges support from an NSF National Young Investigator award.

REFERENCES

Belloni, T., Méndez, M., King, A. R., van der Klis, M., & van Paradijs, J. 1997, ApJ, 488, L109
Chen, W., Shrader, C. R., & Livio, M. 1997, ApJ, 491, 312
Chen, X., & Taam, R. E. 1995, ApJ, 441, 354
Cui, W., Zhang, S. N., & Chen, W. 1998, ApJ, 492, 53
Eikenberry, S. S, Matthews, K., Morgan, E. H., Remillard, R. A., & Nelson, R. W. 1998, ApJ, 494, L61
Fender, R. P., Pooley, G. G., Brocksopp, C., & Newell, S. J. 1997, MNRAS, 290, L65
Greiner, J., Morgan, E. H., & Remillard, R. A. 1996, ApJ, 473, L107
Greiner, J., Predehl, P., & Pohl, M. 1995, A&A, 297, L67
Hameury, J. M., Lasota, J.-P., McClintock, J. E., & Narayan, R. 1997, ApJ, 489, 234
Harmon, B. A., et al. 1995, Nature, 374, 703
Hjellming R. M., & Rupen, M. P. 1995, Nature, 375, 464
Jahoda, K., Swank, J. H., Giles, A. B., Stark, M. J., Strohmayer, T., Zhang, W., & Morgan, E. H. 1996, Proc. SPIE, 2808, 59
Kroeger, R. A., Strickman, M. S., Grove, J. E., Kaaret, P., Ford. E., Harmon, B., & McConnell, M. 1996, A&AS, 120, 117
Kuulkers, E., Wijnands, R., Belloni, T., Méndez, M., van der Klis, M., & van Paradijs, J. 1998, ApJ, 494, 753
Levine, A. M., et al. 1996, ApJ, 469, L33
McClintock, J. E. 1998, in AIP Conf. Proc. 431, Accretion Processes in Astrophysical Systems, ed. S. S. Holt & T. Kallman (New York: AIP), 290
McKay, D., & Kesteven, M. 1994, IAU Circ. 6062
Méndez, M., Belloni, T., &van der Klis, M. 1998, ApJ, 499, L187
Merloni, A., Vietri, M., Stella, L., & Bini, D. 1999, MNRAS, 304, 155
Mioduszewski, A. J., Hjellming, R. M., Rupen, M. P., McCollough, M., Waltman, E. B., & Poolet, G. G. 1997, BAAS, 29, 1387
Mirabel, I. F., Dhawan, V., Chaty, S., Rodríguez, L. F., Martí, J., Robinson, C. R., Swank, J., & Geballe, T. 1998, A&A, 330, L9
Mirabel, I. F., & Rodríguez, L. F. 1994, Nature, 371, 46
Molteni, D., Sponholz, H., & Chakrabarti, S. K. 1996, ApJ, 457, 805
Morgan, E. H., Remillard, R. A., & Greiner, J. 1997, ApJ, 482, 993
Muno, M. P., Morgan, E. H., & Remillard, R. A. 1999, ApJ, 525, in press (astroph/9904087)
Newell, S. J., Garrett, M. A., & Spencer, R. E. 1998, MNRAS, 293, L17
Nowak, M. A., Wagoner, R. V., Begelman, M. C., & Lehr, D. E. 1997, ApJ, 477, L91
Orosz, J. A., & Bailyn, C. D. 1997, ApJ, 477, 876
Orosz, J. A., Remillard, R. A., Bailyn, C. D., & McClintock, J. E. 1997, ApJ, 478, L83
Perez, C. A., Silbergleit, A. S., Wagoner, R. V., & Lehr, D. E. 1997, ApJ, 476 589
Pooley, G., & Fender, R. 1997, MNRAS, 292, 925
Remillard, R. A., Bradt, H., Cui, W., Levine, A. M., Morgan, E. H., Shirey, B., & Smith, D. 1996, IAU Circ. 6393
Remillard, R. A., & Morgan, E. H. 1998, in The Active X-Ray Sky, ed. L. Scarsi, H. Bradt, P. Giommi, & F. Fiore (Amsterdam: Elsevier), 316

Remillard, R. A., Morgan, E. H., McClintock, J. E., Bailyn, C. D., & Orosz, J. A. 1998, in Proc. 18th Texas Symp. on Relativistic Astrophyics, ed. A. Olinto, J. Frieman, & D. Schramm (Singapore: World Scientific), 750
Shahbaz, T., van der Hooft, F., Casares, J., Charles, P. A., & van Paradijs, J. 1999, MNRAS, in press (astro-ph/9901334)
Shapiro, S. L., & Teukolsky, S. A. 1983, Black Holes,White Dwarfs, and Neutron Stars (New York: Wiley)
Shimura, T., & Takahara, F. 1995, ApJ, 445, 780
Smith, D. M., Heindl, W. A., Swank, J., Leventhal, M., Mirabel, I. F., & Rodríguez, L. F. 1997, ApJ, 489, L51
Sobczak, G., McClintock, J. E., Remillard, R. A., Bailyn, C. D., & Orosz, J. A. 1999, ApJ, 520, 776
Tanaka, Y., & Lewin, W. 1995, in X-Ray Binaries, ed. W. Lewin, J. van Paradijs, & E. van den Heuvel (Cambridge: Cambridge Univ. Press), 126
Tavani, M., Fruchter, A., Zhang, S. N., Harmon, B., Hjellming, R. M., Rupen, M. P., Bailyn, C., & Livio, M. 1996, ApJ, 473, L103
Tingay, S. J., et al. 1995, Nature, 374, 141
Titarchuk, L., Lapidus, I., & Muslimov, A. 1998, ApJ, 499, 315
Tomsick, J. A., et al. 1999, ApJ, 512, 892
Ueda, Y., Inoue, H., Tanaka, Y., Ebisawa, K., Nagase, F., Kotani, T., & Gehrels, N. 1998, ApJ, 492, 782
van der Hooft, F., Heemskerk, M. H. M., Alberts, F., & van Paradijs, J. 1998, A&A, 329, 538
van der Klis, M. 1994, ApJS, 92, 511
———. 1995, in X-Ray Binaries, ed. W. Lewin, J. van Paradijs, & E. van den Heuvel (Cambridge: Cambridge Univ. Press), 252
Wagoner, R. V. 1998, in Astrophysical Fluids: From Atomic Nuclei to Stars and Galaxies, in press (astro-ph/9805028)
Zhang, S., Cui, W., & Chen, W. 1997, ApJ, 482, L155
Zhang, S. N., et al. 1997, ApJ, 479, 381
Zhang, W., Jahoda, K., Swank, J. H., Morgan, E. H., & Giles, A. B. 1995, ApJ, 449, 930